Unsuspected Herniated Lung Obstructing the Right Internal Jugular Vein and Internal Carotid Artery in a Patient with Thoracic Outlet Syndrome: MRI/MRA and MRV

James D. Collins, M.D.

Abbreviations: MRI, Magnetic Resonance Imaging; MRA, Magnetic Resonance Angiography; MRV, Magnetic Resonance Venography; TOS, Thoracic Outlet Syndrome

Keywords: lung herniation■thoracic outlet syndrome■migraine■brachial plexus■costoclavicular compression■venous obstruction■internal jugular veins■MRI■MRA■MRV

Correspondence: James D. Collins, M.D., Department of Radiological Sciences, David Geffen School of Medicine at UCLA.

http://dx.doi.org/10.1016/j.jnma.2016.03.001

CLINICAL HISTORY

A 61-year-old, right-handed female complained of tingling and numbness in the ulnar aspect of the left hand eight weeks prior to a second orthopedic evaluation. She had presented twelve years earlier with right neck and shoulder pain. She underwent physical therapy and practiced yoga, with some relief. One year prior to her second evaluation she was a victim of domestic violence and also involved in a motor vehicle accident. Her symptoms progressed to include increased pain over the right neck and both shoulders; episodic headaches; back pain radiating down into both legs; fainting at high altitudes, and tingling and numbness (paresthesias) radiating into the extensor surface of the left arm and down into the 3rd, 4th, and 5th fingers of her left hand. Electromyography and nerve conduction studies were positive for mild sensory C8/T1 dysfunction, but negative for left cervical radiculopathy or brachial plexopathy. Physical examination revealed blood pressure 110/70, pulse 72, and temperature at 36.5 C; forward rotated shoulders, right drooped as compared to left; tenderness to palpation over the base of the left neck and supraclavicular fossa, and complaint of pain when the neck was turned to the right or to the left. The requesting neurologist suspected thoracic outlet syndrome (TOS), left greater than right, and requested bilateral MRI/MRA and MRV of the brachial plexus to determine site(s) of costoclavicular compression.[1]

METHODS AND MATERIALS

Plain chest radiographs (PA and lateral) are obtained and reviewed prior to the MRI. The procedure is discussed and the patient examined. Respiratory gating is applied throughout the procedure to minimize motion artifact. The patient is supine in the body coil, arms down to the side and imaging is monitored at the MRI station. Magnetic resonance images are obtained on the 1.5 Tesla GE Signa XL MR scanner (GE Medical Systems, Milwaukee, Wisconsin). A body coil is used and no intravenous contrast agents are administered. A saline water bag is placed on the right and the left side of the neck to increase signal to noise ratio for high-resolution imaging. A full field of view (44 cm) of the head, neck and thorax is used to image both supraclavicular fossae. Contiguous (4 mm) coronal, transverse (axial), oblique transverse, sagittal, and abduction external rotation of the upper extremities (AER) T1-weighted images, and 2D Time Of Flight (TOF) MRA/MRV are obtained. If there is clinical evidence of scarring, tumor and/or lymphatic obstruction, Fast Spin Echo T2-weighted images are selectively obtained. The parameters for acquiring each sequence have been published.

CHEST RADIOGRAPHS AND MAGNETIC RESONANCE FINDINGS

The Posterior Anterior (PA) chest radiograph (Fig. 1) displays the anterior rotated heads of the clavicles (C) over the posterior 3rd ribs; drooping right shoulder and coracoid process (CP) as compared to the elevated left shoulder and scapula, reflecting rounding shoulders; left first rib (FR) and clavicle higher than right, and mild right concave scoliosis of the thoracic spine, greatest at the level of T5-T12 vertebrae; left transverse process of the left T1

Figure 1. PA chest radiograph displays an area of increased radiolucency (white arrows) that overlies the trachea (T), displaced to the left of midline; anterior rotated clavicles (C); horizontal density at the right costophrenic sulcus (X), reflecting old inflammatory disease. Observe the mild concave left thoracic spine scoliosis, T5-T12, A, aorta; CP, coracoid process; FR, first rib; LV, left ventricle; 5T, fifth thoracic vertebra; 9T, ninth thoracic vertebra.

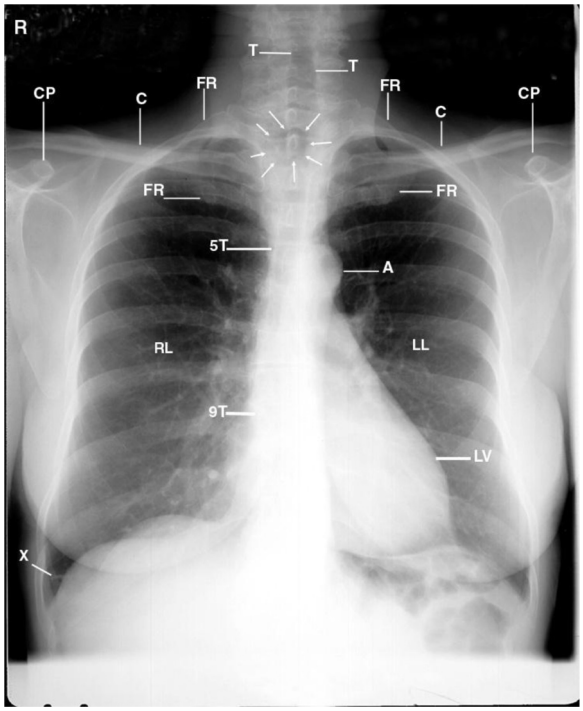

Figure 2. Lateral chest radiograph displays mild anterior bowing of the body of the sternum (S), backward displaced manubrium (M), mild kyphosis of the thoracic spine (7T), and rounding of the shoulders (X). A, aorta; T, trachea; LV, left ventricle, Seventh thoracic vertebra, 7T.

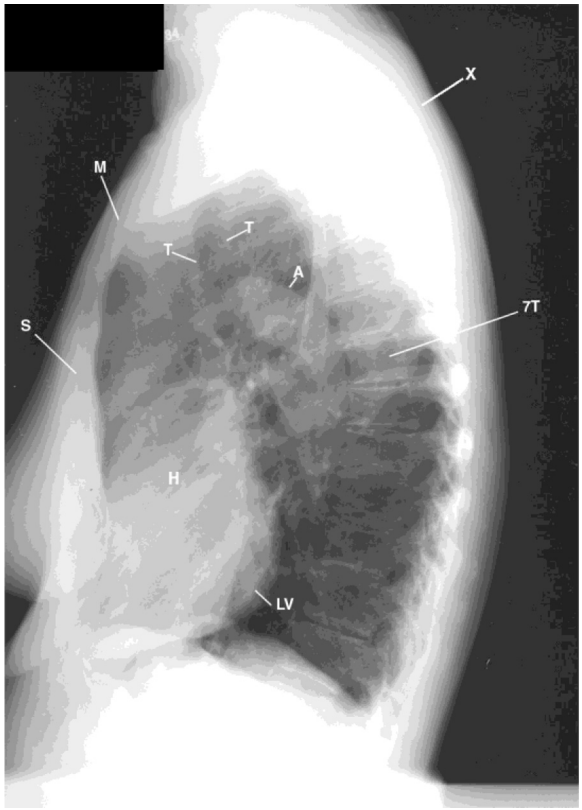

vertebra higher than the right, and the elongated transverse process of the right C7 vertebra crossing the transverse process of the first thoracic vertebra. A linear horizontal dense scar (X) overlays the irregular right costophrenic sulcus, reflecting old inflammatory disease. An oval area of low density (arrows) overlays the trachea extending right of midline, at the level of the second thoracic vertebra with concave displacement of the trachea to the left of midline.

The lateral chest radiograph (Fig. 2) displays thin subcutaneous tissues; anterior bowed body of the sternum (S) with the backward manubrium (M), and right kyphoscoliosis of the thoracic spine increasing the slopes of the first ribs, left lower than right, and rounding of the shoulders (X).[2]

CONCLUSION(S) FOR THE CHEST RADIOGRAPHS

1. Bilateral rounding of the shoulders, left greater than right.
2. Radiolucency over second thoracic vertebra, possible lung herniation.
3. Mild right concave kyphoscoliosis thoracic spine.
4. Scarring right lung base.

MAGNETIC RESONANCE IMAGING FINDINGS

The coronal MRI sequence (Fig. 3A) cross-referenced the PA chest radiograph to display an area of low proton density (HL) over the right thoracic inlet. A right lung herniation or a vascular abnormality was considered the most likely etiologies.[3,4] Therefore, the two-dimensional Time Of Flight (2D TOF) MRA/ MRV sequence was acquired out of routine order to determine whether the abnormal low proton density was vascular or lung in origin (Fig. 4A). The expanded low proton density (HL) on the coronal T1 weighted image (Fig. 3A) proved not to be vascular in origin. The diagnosis of cervical lung herniation was made. The transverse, transverse oblique (not displayed), and the sagittal sequences crossed referenced costoclavicular compression of the vascular supply as displayed on the coronal sequence. Sequential

Figure 3. (A) Coronal T1-weighted image in the neutral position displays the patient leaning left reflecting guarding of the atrophic left shoulder; low proton dense herniated right lung (HL) displacing the esophagus (E), trachea (T), right common carotid artery (CC), and the gray proton dense left brachiocephalic vein (BRV) laterally; costoclavicular compression of left axillary artery (not labeled) on the cephalic vein (CV) as it drains into axillary vein (AXV) impeding venous return; intermediate high proton dense turbulence within the left internal jugular vein (J); gray proton dense dilated right axillary vein (AXV) reflecting impedance to venous return into the compressed gray proton dense region of the inferior bicuspid valve of the right internal jugular vein (J) as it drains into the compressed right brachiocephalic vein (not labeled). A, aorta; AS, anterior scalene muscle). (B) Coronal abduction external rotation (AER) of the upper extremties T1-weighted image enhances costoclavicular compression as described in Figure 3A reflected by the concave depression of the axillary veins (AXV) by the clavicles (C) and subclavius muscles (SUB). Observe the dilatation of the right transverse cervical artery (TCA) and the gray proton dense left external jugular vein (XJ) enhancing impedance to arterial flow and impedance to venous return into the compressed left subclavian vein (SV). A, aorta; AS, anterior scalene muscle; BR, brachiocephalic artery; CC, common carotid artery; CV, cephalic vein; D, deltoid muscle; E, esophagus; HL, herniated lung; FR, first rib; BRV, brachiocephalic vein; J, internal jugular vein: LL, left lung; RL, right lung; SA, subclavian artery; STM, sternocleidomastoid muscle; T, trachea.

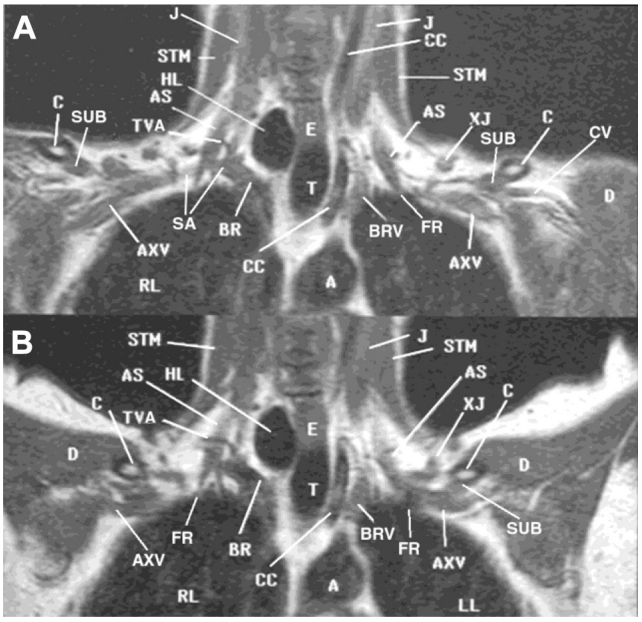

Figure 4. (A) Coronal 3D reconstructed 2D TOF MRA/ MRV in the neutral position displays the mildly dilated gray proton dense impedance to arterial flow in the right subclavian artery (SA) reflecting costoclavicular compression of the right axillary artery (AX) and the markedly decreased proton dense venous return in the compressed right subclavian vein (SV). Observe the gray proton dense compressed descending right internal jugular vein (X) and the ascending right common carotid artery (CC) and the medial concave displacement of the right carotid sheath corresponding to right lateral displacement by the herniated lung as displayed on the T1 weighted image in Figures 3A and 3B; decreased proton density of the compressed bicuspid valve in the left subclavian vein accentuating the high proton dense impedance to venous return in the dilated high proton dense left external vein as compared to the right external jugular vein. (B) Displays abduction external rotation of the upper extremities displayed in Figure 4A enhancing costoclavicular and coracoid compression of the vascular supply to the upper extremities. Observe the diminished proton densities of the axillary arteries (AX) and veins (AXV), proximally dilated gray proton dense descending left internal jugular vein draining into the higher proton dense left brachiocephalic vein and the dominate descending left internal jugular vein (J) as compared to the right, and the enhanced compression of the left carotid sheath as compared to Figure 4A. A, aorta; BR, brachiocephalic artery; CC, common carotid artery; CV, cephalic vein; BRV, brachiocephalic vein; J, internal jugular vein, LTV, long thoracic vein; SVC, superior vena cava; VA, vertebral artery; VV, vertebral vein; W, water bag; XJ, external jugular vein.

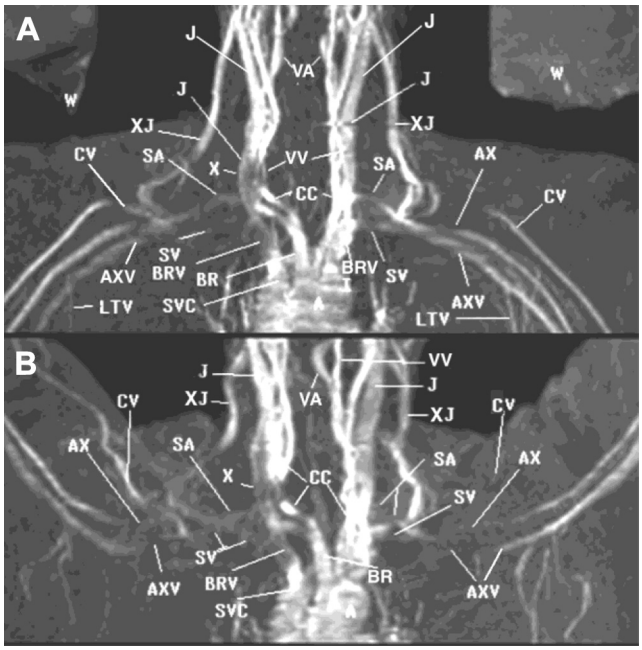

transverse images (Fig. 5, Images 21−24) displayed right lung herniation (HL); displacement of the trachea (T) and esophagus (E) to the left of midline; anterior lateral concave displacement of the right carotid sheath (J, CC); splaying apart right vagus (V) and recurrent laryngeal (RE) nerves; left anterior scalene muscle (AS), larger than right, compressing the second division of the tense left subclavian artery (SA), and the dilated vertebral veins reflecting impedance to venous return, left greater than right. The right sagittal neutral position (Fig. 6A) displays the anterior rotated head of the right clavicle (C) against the region of the inferior bicuspid valve within the right internal jugular vein (J) against the first division of the right subclavian artery (SA)[5]; low proton dense right herniated lung (HL), and costoclavicular compression of the subclavian and axillary veins, left greater than right (not displayed on this image). The left sagittal sequence (not displayed) cross-referenced the coronal sequence and displayed greater costoclavicular compression of the bicuspid valve within the dilated left external jugular vein as it drained over the bicuspid valve within the compressed left subclavian vein on the first rib; costoclavicular compression of the left cephalic vein on the bicuspid valve within the left axillary vein, and high proton dense left chest wall veins reflecting divergence of venous return as compared to the lower proton densities in the right chest wall veins.[6]

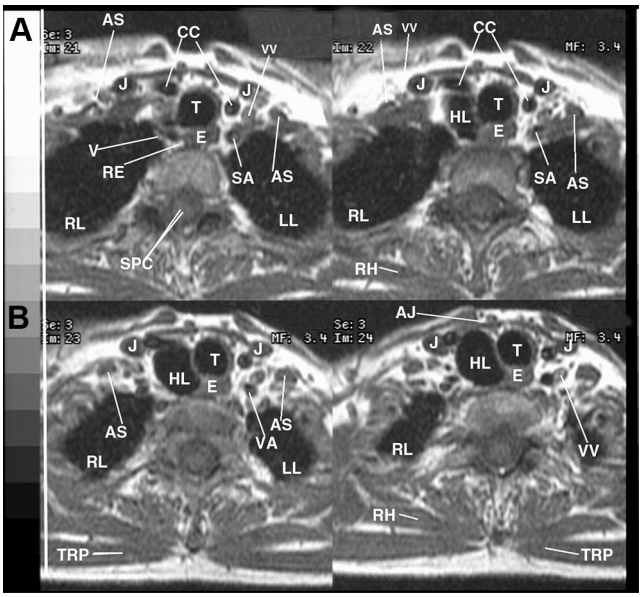

Figure 5. (A) (images 21-24). Sequential transverse images display the herniated lung (HL) displacing the right vagus nerve (V) laterally (image 21). It also displaces recurrent nerve (RE) with the esophagus (E) and trachea (T) to the left of midline **(images 21 and 22)**. The herniated lung expands anteriorly to compress the right common carotid artery (CC) and the jugular vein **(B) (images 23 and 24)**. Observe the tense left subclavian artery (SA) posterior to the larger left anterior scalene muscle (AS) (image 22) and the dilated left vertebral artery and vein (images 22 and 24). LE, levator scapulae muscle; LL, left lung; RL, right lung; SPC, spinal cord; TRP, trapezius muscle; XJ, external jugular vein.

The coronal neutral 3D reconstructed 2D TOF MRA/MRV sequence (Fig. 4A) cross referenced the coronal T1 weighted sequence to display the region of the right herniated lung (X) medially compressing the right carotid sheath laterally and the anterior rotated clavicle with the backward sternocleiodmastoid muscle compressing the inferior bicuspid valve within right internal jugular vein against the right vertebral vein (VV) against and the anterior scalene muscle, evident by the diminished proton densities within the right internal jugular vein (J) and the common carotid artery (CC); proximal dilatation of the right axillary vein (AXV), and poststenotic reciprocal high proton dense dilated right axillary artery (not labeled) reflecting the site of right costoclavicular compression as compared to the greater costoclavicular compression of the venous drainage on the left. The diminished proton densities within the second and third divisions of the right subclavian (SA) and axillary (AX) arteries reflect costoclavicular compression from impedance to forward arterial flow. The diminished proton densities within the second division of the left subclavian artery (SA) with binding nerve trunks, and the proximally dilated high proton dense left external jugular vein (XJ) as it drains compressed on the left subclavian vein (SV) with diminished proton density reflected costoclavicular compression of the draining veins within the neck and supraclavicular fossa (Fig. 4A). The diminished proton density of the costoclavicular compressed left axillary artery (AX) on the axillary vein (AXV) and the proximal high proton dense left brachiocephalic vein compressed by the backward manubrium against the ascending aorta reflected greater costoclavicular compression within the draining veins of the left neck, and supraclavicular fossa as compared to the right.

The bilateral coronal abduction external rotation (AER) T1-weighted sequence (Fig. 3B) displayed posterior inferior rotation of the clavicles (C) with the subclavius muscles (SUB); backward displaced manubrium (not displayed), and the posterior anterior medial rotation of the coracoid processes with attached muscles (not displayed) enhancing costoclavicular compression of the draining veins and lymphatics within the neck and supraclavicular fossae with lymphatics and mild compression of the neurovascular bundles (subclavian and axillary arteries with binding nerves) left greater than right. The decreased in venous return increased intrathoracic pressure further expanding the fascial plane of the herniated lung (HL) as compared to the neutral coronal sequence (Fig. 3A). The right sagittal abduction external rotation sequence (Fig. 6B) crossed referenced the coronal abduction sequence to display the backward displaced clavicle (C) with the backward sternocleidomastoid muscle on the manubrium (M) compressing the region of the inferior bicuspid valve in the right internal jugular vein (not labeled) against the herniated lung (HL); dilatation of the superior vena cava (SVC), azygos vein (AZ), and right internal jugular (J) vein proximal to the inferior bicuspid valve, expanded low proton dense herniated right lung (HL), and the internal thoracic vein (IN) (Fig. 6B).

The coronal abduction external rotation 3D reconstructed 2D TOF MRA/MRV sequence (Fig. 5B) cross-referenced the T1 weighted coronal abduction external rotation sequence to display enhanced costoclavicular compression of the draining veins (J, SV, AXV) within the neck and supraclavicular fossae, and the neurovascular bundles, left greater than right. The bilateral arms overhead maneuver (AER) sequence enhanced right lung herniation and costoclavicular compression, evident by dilatation of the common carotid arteries (CC), internal jugular veins (J) proximal to the region of the inferior bicuspid valves, left greater than right, and proximal dilatation of the axillary veins lateral to the region of the anterior medial rotated coracoid processes.

Bilateral coronal abduction external rotation of the upper extremities (AER) position triggered complaints of

Figure 6. (A) Right sagittal image in neutral position displays compression of the region of the right carotid sheath anterior laterally by the low proton dense herniated lung (HL). Observe the backward displaced manubrium (M) to 35° off the vertical axis reflecting rounding of the shoulder. (B) Right sagittal image abduction external rotation (AER) with arms overhead. Displays enhanced costoclavicular compression of the draining veins within the neck and mediastinum. Observe the dilated right brachiocephalic (BRV) vein, left internal jugular and azygos veins (AZ) and the superior vena cava (SVC). The manubrium is further displaced posteriorly to 42°. Observe the posterior rotation of the right clavicle (C) compressing the region of the inferior bicuspid valve within the right internal jugular against the dilated first division of the subclavian artery (SA) and dilatation of the pulmonary veins and the superior vena cava as compared to Figure 6A. There is enhanced dilatation of the herniated lung reflecting increased intrathoracic pressure. AJ, anterior jugular vein; AS, anterior scalene muscle; CC, common carotid artery; E, esophagus; BRV, brachiocephalic vein; RA, right atrium; STM, sternocleidomastoid muscle.

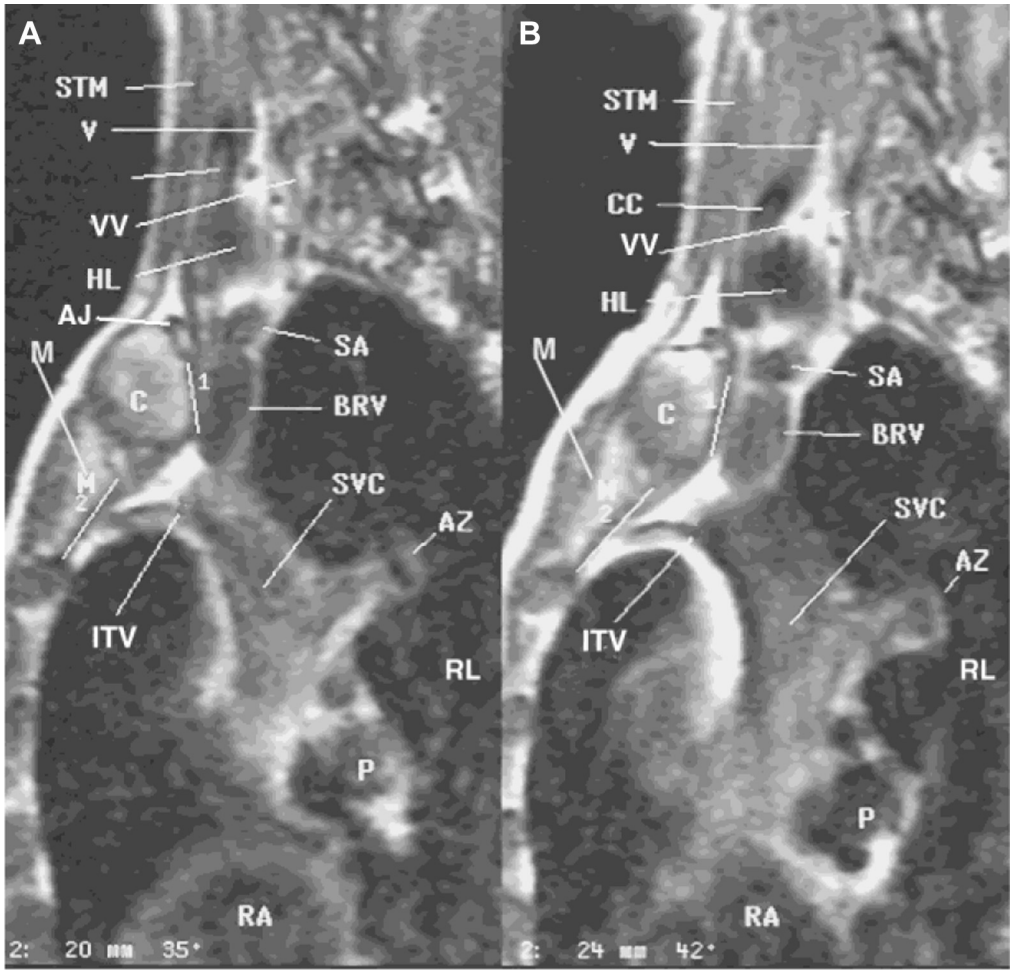

deep pressure sensation over the right neck, shoulder, and arm.[2] Left sided triggered complaints consisted of pain in the left neck and shoulder; tingling and numbness in the left arm and hand, left-sided occipital headache, and complaint of dizziness that persisted long after leaving the MRI gantry.

The images acquired with the described findings above were reviewed with the patient on completion of the procedure. Selected annotated images were provided for the referring physician. She was advised to follow-up with her referring physician. Following evaluation by a thoracic surgeon, the patient was deemed not to be a surgical candidate. She was advised to undergo physical therapy for thoracic outlet syndrome by a qualified physical therapist.

MRI DIAGNOSTIC FINDINGS

1. Bilateral rounding of the shoulders, left greater than right.
2. Mild right concave kyphoscoliosis thoracic spine caused asymmetric increase in the sloped of the first ribs.
3. Right lung herniation in the right scalene triangle enhanced compression of the inferior bicuspid within valve the right internal jugular vein. See Detailed Description Above.
4. Backward manubrium with body of the sternum compressed the gray proton dense left brachiocephalic vein against the ascending aorta decreasing venous return from the left head and neck, and the

left supraclavicular fossa greater left than on the right.

5. Bilateral costoclavicular compression (laxity of the sling/erector shoulder muscles-trapezius, levator scapulae, serratus anterior) of the bicuspid valves within the draining veins of the neck, supraclavicular fossae with lymphatics, and compression of the subclavian and axillary arteries with binding nerves, left greater than right.
6. 2D Time Of Flight MRA and MRV confirmed costoclavicular compression secondary to the high proton dense left brachiocephalic vein greater than on the right. See Detailed Descriptions Above.[1]
7. Bilateral coronal abduction external rotation (AER) of the upper extremities triggered complaints of deep pressure sensation over the right neck, shoulder, and arm. Left triggered complaints consisted of pain in the left neck and shoulder with tingling and numbness in the left arm and hand, left side occipital headache, and dizziness that persisted long after she left MRI gantry.

DISCUSSION

Herniation of the lung is the protrusion of lung beyond the normal boundaries of the thorax, which is accentuated by increased intrathoracic pressure.[3] In the thoracic inlet, a thin layer of deep neck fascia known as Sibson's fascia normally limits protrusion of the lung. This fascia envelopes the neurovascular supply of the upper extremity and forms fascial planes from the root of the neck to the lower part of the axilla. It covers and reinforces the apex of the lung, as it extends from the transverse processes of the seventh cervical vertebra to the inner border of the first rib.[1] Congenital/traumatic defects in Sibson's fascia allows the lung to protrude through the thoracic inlet, commonly between the sternocleidomastoid and anterior scalene muscles.[5] Complications of cervical lung hernia are rare, and include airway obstruction, and transient venous occlusion.

Cervical hernias may be diagnosed by physical examination, chest radiographs or computerized tomography (CT). Conventional X-ray, linear tomography, CT and magnetic resonance imaging (MRI) are radiographic modalities used to image the thorax, shoulder girdle and soft tissues. Conventional X-ray techniques incompletely image vascular structures, surface anatomy and soft tissues. Gray scale applied to CT extends the capabilities of x-ray imaging to obtain detailed transverse anatomic sections. However, CT does not definitively separate tumors from vascular and/or neurovascular structures within fascial planes. Detailed peripheral imaging in fascial planes is not possible by CT. Magnetic resonance imaging (MRI) displays soft-tissue detail by proton density distribution; provides high resolution imaging of nerves, vascular structures and the lymphatics; separates proton densities within organ systems, and does not require reconstruction or repositioning of the patient.[2] Monitored multi-planar MRI displays the anatomy of the brachial plexus and peripheral nerves for investigation by sequential imaging of landmark anatomy according to proton density distribution. Magnetic resonance angiography (MRA) and venography (MRV) display vascular anatomic detail of neck, thorax, and shoulder girdle. Sunderland's 1945 anatomic nerve model demonstrated the blood supply (microcirculation) of nerves.[5] A gross anatomic nerve model of the brachial plexus demonstrated the MRI of the vascular supply as low proton densities marginating nerves, that contributes to the separation of nerves from surrounding tissues.[1] This manuscript applies the knowledge of landmark anatomy and of MRI, MRA and MRV to display compromising abnormalities of the thoracic inlet, which correlate with the patients' clinical complaints. This presentation displays bilateral MRI, MRA and MRV of the brachial plexus at the time of the unsuspected cervical lung herniation in a 61-year-old woman with thoracic outlet syndrome. This technique demonstrates costoclavicular compression of the bicuspid valves within veins of the neck and supraclavicular fossae, lymphatics, and the neurovascular bundles. Each sequence provided multiple images. All sequences and images were cross-referenced in order to arrive at an accurate diagnosis.

Since it is not possible to present all of the acquired images, the images selected for this presentation were annotated to best display the pathology. This patient had a long history of the right neck and shoulder pain that responded to conservative physical modalities and yoga as advised by her first orthopedist. One year prior to her second orthopedic evaluation she sustained injuries in a motor vehicle accident and injuries as a result of domestic violence, which significantly accelerated her right-sided musculoskeletal symptoms. She presented with the addition of neural and vasculature complaints that were consisted with thoracic outlet syndrome (TOS): bilateral neck, shoulder, and arm pain; numbness and tingling of the hands, especially the ulnar aspect of the left hand; new onset of headache, and syncopal episodes while at high altitude. The PA and lateral chest radiographs displayed bilateral round shoulders, left concave kyphoscoliosis of the thoracic spine, right lung base scarring, and a radiolucency over the right neck of unknown etiology. She then underwent definitive MRI, MRA and MRV of the brachial plexus that confirmed TOS with bilateral costoclavicular

compression of the bicuspid valves within the internal jugular and subclavian veins in the neck and supraclavicular fossae with lymphatics, and neurovascular bundles in the neutral position, left greater than right.[2] Unexpectedly, she was found to have right lung herniation that compressed the right carotid sheath (Figs. 3A, 4). The abduction external rotation (stress) sequence posteriorly displaced the Manubrium with body of the sternum and the clavicles with subclavius muscles (Figs. 3B, 6B) that increased intrathoracic, intraabdominal, and intracranial pressures.[7] This arm overhead maneuver enhanced costoclavicular compression, triggered the patient's TOS symptoms, and captured images, which provided functional anatomic correlation of the presenting complaints. The patient's history of repeated trauma resulted in postural and mechanical changes that increased laxity of the shoulder muscles. Our thoracic outlet syndrome data confirms patients present with tingling, numbness, and pain over the upper and lower extremities, headache, dizziness, visual disturbances, and rounding of the shoulders. Coronal abduction external rotation (AER) sequence with the arms fully extended overhead within the MRI gantry triggered complaints.

Our patient presented with TOS symptoms, pain and muscle spasms, and laxity of the sling/erector muscles (trapezius, levator scapulae, and the serratus anterior muscles). The laxity of the sling/erector muscles increased the asymmetric slope of the first ribs that causes backward displacement of the manubrium with the clavicles and sternocleidomastoid muscles and compression of the soft tissues within the neck and supraclavicular fossae. Without adequate treatment and increasing age, kyphosis of the thoracic spine further shifts shoulders forward and enhances costoclavicular compression.

The authors are aware of alternative diagnoses that may have caused her complaints, but none of these were found. We are also aware that out narrative presentation included statements without all the images displayed. The patient's permanent file contains a detailed report of all of the acquired images in each sequence. Unlike x-ray images, a diagnosis is not made from a single film. Because it was not possible to present all of the images, those selected best demonstrated the pathology.

TAKE HOME MESSAGE

The knowledge of the clinical history, anatomy, physiology, and that the circulatory system is a closed system is essential in making an accurate diagnosis. Any decrease in venous return increases intrathoracic, intracranial, and intraabdominal pressure that triggers patient complaints as in our patient.[7] Since nerves bind to an artery to receive their nutrients and lymphatics on veins return waste and venous blood back into the circulation, you can't compress a nerve without compressing the blood supply.[1]

Baseline posterior anterior and lateral chest radiographs are essential for examination of the thorax on MRI, MRA and MRV of the brachial plexus. Upright chest x-rays provide display of 70% of normal and abnormal landmark anatomy because 30% of the x-ray beam is absorbed by the patient. It is important for the imaging of the chest that the cervical spine be displayed up-to the 5th cervical vertebra for detection of cervical ribs, anomalies and degenerative changes of the cervical spine. The detected lucency over the cervical spine alerted the radiologist to change protocol for bilateral MRI, MRA, and MRV of the brachial plexus. Monitored magnetic resonance imaging and the knowledge of landmark anatomy allows the radiologist to consider different etiologies in patient care prior to completion of procedures. This presentation stresses the importance of obtaining baseline plain radiographs before Magnetic resonance imaging/CT imaging as landmark abnormalities/ anomalies are often missed by the radiologist.

REFERENCES

1. Collins, J. D., Saxton, E., Miller, T. Q., Ahn, S. S., Gelabert, H., & Carnes, A. (1995). Compromising abnormalities of the brachial plexus as displayed by Magnetic resonance imaging. *Clinical Anatomy, 8*, 1–16.
2. Collins, J. D., Saxton, E., Miller, T. Q., Ahn, S. S., Gelabert, H., & Carnes, A. (2003). Scheuermann's disease as a model displaying the mechanism of venous obstruction in thoracic outlet syndrome and migraine patients: MRI and MRA. *J Nat Med Assoc, 95*, 298–306.
3. Ross, R. T., & Burnett, C. M. (1999). A traumatic lung herniation. *Ann Thorac Surg, 67*, 1496–1497.
4. Rusca, M., Carbognani, P., Cattelani, L., Tincani, G., & Bobbio, P. (2000). Spontaneous intercostal pulmonary hernia. *J Cardiovasc Surg, 41*, 641–642.
5. Sunderland, S. 1968. Nerves and Nerve Injuries, Baltimore, Williams & Wilkins Co. 8. www.tosinfo.com *Thoracic Outlet Syndrome (TOS) Information*. Website designed by Ramona Tung, 2002.
6. Woodburne, R. T., & Burkel, W. E. (1988). *Essentials of Human Anatomy* (Ed 8th, 18–216). New York: Oxford University Press.
7. Clemente, C. D. (2007). *Anatomy: A Regional Atlas of The Human Body* (Ed. 5). Lippincott, Williams, and Wilkins, 3. Collins JD, Shaver ML, Disher AC, Miller TQ. 1995b.